Spectral line shapes in linear absorption and two-dimensional spectroscopy with skewed frequency distributions

Farag, Marwa H.; Hoenders, Bernhard J.; Knoester, Jasper; Jansen, Thomas L. C.

Published in:
Journal of Chemical Physics

DOI:
10.1063/1.4985665

Spectral line shapes in linear absorption and two-dimensional spectroscopy with skewed frequency distributions

Marwa H. Farag, Bernhard J. Hoenders, Jasper Knoester, and Thomas L. C. Jansen

Citation: The Journal of Chemical Physics **146**, 234201 (2017);
View online: https://doi.org/10.1063/1.4985665
View Table of Contents: http://aip.scitation.org/toc/jcp/146/23
Published by the American Institute of Physics

Spectral line shapes in linear absorption and two-dimensional spectroscopy with skewed frequency distributions

Marwa H. Farag, Bernhard J. Hoenders, Jasper Knoester, and Thomas L. C. Jansen[a)]
Zernike Institute for Advanced Materials, University of Groningen, Nijenborgh 4, 9747 AG Groningen, The Netherlands

(Received 3 March 2017; accepted 31 May 2017; published online 19 June 2017)

The effect of Gaussian dynamics on the line shapes in linear absorption and two-dimensional correlation spectroscopy is well understood as the second-order cumulant expansion provides exact spectra. Gaussian solvent dynamics can be well analyzed using slope line analysis of two-dimensional correlation spectra as a function of the waiting time between pump and probe fields. Non-Gaussian effects are not as well understood, even though these effects are common in nature. The interpretation of the spectra, thus far, relies on complex case to case analysis. We investigate spectra resulting from two physical mechanisms for non-Gaussian dynamics, one relying on the anharmonicity of the bath and the other on non-linear couplings between bath coordinates. These results are compared with outcomes from a simpler log-normal dynamics model. We find that the skewed spectral line shapes in all cases can be analyzed in terms of the log-normal model, with a minimal number of free parameters. The effect of log-normal dynamics on the spectral line shapes is analyzed in terms of frequency correlation functions, maxline slope analysis, and anti-diagonal linewidths. A triangular line shape is a telltale signature of the skewness induced by log-normal dynamics. We find that maxline slope analysis, as for Gaussian dynamics, is a good measure of the solvent dynamics for log-normal dynamics. *Published by AIP Publishing.* [http://dx.doi.org/10.1063/1.4985665]

I. INTRODUCTION

Two-dimensional correlation spectroscopy (2DCS) for electronic[1] (2DES) and infrared[2] (2DIR) optical transitions has been extensively applied to extract real-time dynamical information in systems of relevance in physics, chemistry, biology, and material science. This spectroscopic technique is closely related to the more established two-dimensional nuclear magnetic resonance correlation spectroscopy technique[3] (COSY). The 2D spectra are generated from a pulse sequence that interacts three times with the sample at different times, t_1, t_2, and t_3.[4,5] By varying the time t_2, the frequency of an oscillator can be measured at two times t_1 and t_3, and the dynamics information can be probed by correlating the initial frequency with the final frequency. Moreover, 2D spectroscopy allows the determination of coupling between different transitions[6] and is sensitive to spectral diffusion due to solvent fluctuations[7–12] and chemical exchange.[13–19] The resulting line shapes can to a first approximation be well understood by the well-established Kubo line shape theory,[4,7,20–22] which, for example, allows the extraction of solvent relaxation times by analyzing the slope,[10,23] ellipticity of the spectral peaks,[24] or through comparison of rephasing and non-rephasing amplitudes.[25] This analysis relies on the fundamental assumption that the underlying solvent dynamics is Gaussian. It has, however, become increasingly evident that this assumption is not accurate for systems involved in hydrogen bonding[26–28] or embedded in a protein matrix.[29,30] This calls for alternative approaches for interpreting the spectral line shapes in these systems. Explicit spectral simulations based on molecular dynamics simulations provide useful insights into these cases.[26–28,31–39] However, more elementary models that can catch the essential dynamics in such systems should provide fundamental insight and are, thus, desirable. In this paper, we will consider three models, which all give rise to non-Gaussian frequency distributions.

In spectroscopic studies, notable non-Gaussian line shapes, in linear and non-linear spectra, have been reported for a number of systems, such as water,[26,27,40–42] photocatalysts,[43] and light harvesting complexes.[29,30] Among these studies, spectral line shapes with a log-normal distribution have been addressed for different systems such as bacteriorhodopsin, light-harvesting complex LH2, and auramine.[44–53] In combined molecular dynamics simulations and semi-empirical electronic structure calculations, the frequency distribution of the Q_y transition in chlorophyll was found to be distributed in a log-normal like fashion.[30] The origin of such skewed spectral shapes was recently studied theoretically.[54] Furthermore, the log-normal distributions are quite common in nature.[55,56] From a theoretical point of view, different models have been constructed to account for the non-Gaussian effect[12,29,57–61] and to investigate the spectral line shape of the time evolution of 2DCS. However, so far no systematic study of the effect of dynamics on the 2DCS has been reported for cases where the underlying frequency distribution is skewed. The purpose of this paper is to investigate the effect of dynamics with non-Gaussian frequency distributions on the line shape and its time evolution in 2DCS and identify the

a)t.l.c.jansen@rug.nl

signature of the skewness on the 2D spectra. To this end, we use three different models to produce frequency trajectories with a skewed distribution. The first model assumes an anharmonic bath mode, the second model assumes two nonlinearly coupled bath coordinates, while the final model is a minimal parameter model assuming log-normal dynamics. The 2D spectra are then calculated and analyzed in terms of the maxline slope and the frequency dependent anti-diagonal width. Finally, the effect of the skewness value on the 2D spectral line shape is systematically analyzed by comparing different log-normal models with varying skewness and comparing with a standard Gaussian model where the skewness is zero.

This paper is organized in the following way. In Sec. II, we describe the methods for constructing frequency trajectories with the different models. In Sec. III, we present and discuss the results. Finally, we draw conclusions in Sec. IV.

II. THEORY

To investigate the spectral line shapes resulting from different models with skewed frequency distributions, equilibrium frequency trajectories $\omega(t)$ were generated. We considered three model systems to produce frequency trajectories. This allowed us to analyze the effect of the skewness term on the linear absorption and 2D spectra in a controlled manner. Specifically, the model Hamiltonian of the quantum system was given by

$$H(t) = (\omega_{01} + \omega(t))B^{\dagger}B, \tag{1}$$

where ω_{01} is the average transition frequency from the ground state to the excited state, and $B^{\dagger}$ and B are the bosonic creation and annihilation operators. The time evolution of the equilibrium frequency was calculated as

$$\omega(t) = c\,x(t), \tag{2}$$

where c defines the strength of the coupling between the system and the bath coordinates $x(t)$. The bath coordinates were generated numerically by using a classical Langevin equation and a random force $R(t)$,[5,62]

$$\frac{d^2x}{dt^2} = -\frac{1}{m}\nabla V(x) - \gamma\frac{dx}{dt} + \frac{1}{m}R(t). \tag{3}$$

Here, m is the mass, $V(x)$ is a potential of mean force, and γ is the friction coefficient. $R(t)$ is a Gaussian random force with

$$\langle R(t)\rangle = 0, \qquad \langle R(0)R(t)\rangle = 2mk_BT\delta(t), \tag{4}$$

where k_B is the Boltzmann constant and T is the temperature. For all models, m was set to unity and the temperature to 300 K.

To generate a bath coordinate with a skewed distribution, three different models were considered. In the first model (AH), the skewness was introduced through an anharmonicity of one of the coordinates. The anharmonic potential was chosen such that it has only one additional parameter (A) to define the anharmonicity and it is bounded,[42,60]

$$V_{\mathrm{AH}}(x_f, x_s) = k_f\,x_f^2/2 + k_s^3\,(e^{A\,x_s/k_s} - A\,x_s/k_s)/A^2, \tag{5}$$

where x_f and x_s are a fast and a slow solvation coordinate as originally introduced in Refs. 42 and 60. The second model (NL) introduced the skewness through a nonlinear coupling between two bath coordinates. The nonlinear coupling was chosen to include only one additional parameter (A) to define the nonlinear coupling,[42,60]

$$V_{\mathrm{NL}}(x_f, x_s) = k_f\,x_f^2/2 + k_s\,x_s^2/2 + k_f\,x_f^2(e^{A\,x_s/k_f} - 1)/2\,. \tag{6}$$

The third model (LN) treated the dynamics on a harmonic potential

$$V(x_s) = k_s\,x_s^2/2, \tag{7}$$

but assumed that the frequency dependence on the bath coordinate is given by an exponential relation with one additional parameter resulting in a log-normal frequency distribution,

$$y_s(t) = \exp(\varrho + \eta x_s(t)), \tag{8}$$

where η is unitless and the coordinate trajectory $x_s(t)$ has a Gaussian distribution with zero average and variance given by $2mk_BT/\Delta t$.

The parameters of the Hamiltonian and the Langevin simulation are summarized in Table I. To simplify the 2D line shape analysis, the parameters for the three models were selected such that the linear absorption spectrum and the frequency fluctuation correlation function are similar (see Sec. III).

The time evolution of the equilibrium frequency $\omega_{\mathrm{AH}}(t), \omega_{\mathrm{NL}}(t)$, and $\omega_{\mathrm{LN}}(t)$ for the AH, NL, and LN models, respectively, was given by

$$\omega_{\mathrm{AH}}(t) = c_f\sqrt{k_f/k_BT}\,x_f(t) + c_s\sqrt{k_s/k_BT}\,x_s(t), \tag{9}$$

$$\omega_{\mathrm{NL}}(t) = c_f\sqrt{k_f/k_BT}\,x_f(t) + c_s\sqrt{k_s/k_BT}\,x_s(t), \tag{10}$$

$$\omega_{\mathrm{LN}}(t) = c_s\,y_s(t). \tag{11}$$

The coordinate distributions for the three models obtained from the Langevin simulation are presented in Fig. 1. While the coordinate x_s for model AH and the coordinates x_f and x_s for model NL are asymmetric with a tail extending toward lower values (negative values), the coordinate y_s for model LN is asymmetric with a tail extending toward higher values (positive values).

The Langevin simulations were run for 100 ns with a time step (Δt) 10 fs and the data were stored every 10 fs. The numerical integration of the Schrödinger equation (NISE)[63,64] scheme

TABLE I. The values of the parameters used for the numerical calculation.

Parameter	Model AH	Model NL	Model LN
γ (ps^{-1})	6.0	20	20
k_f (k_BT)	100	100	...
k_s (k_BT)	3.6	3.6	3.6
c_f (cm^{-1})	–2.1	–2.7	...
c_s (cm^{-1})	–21.3	–24.0	67.0
A (k_BT)	10	250	...
ω_{01} (cm^{-1})	1507	1499	1450
ϱ	...	...	0.0
η	...	...	0.8

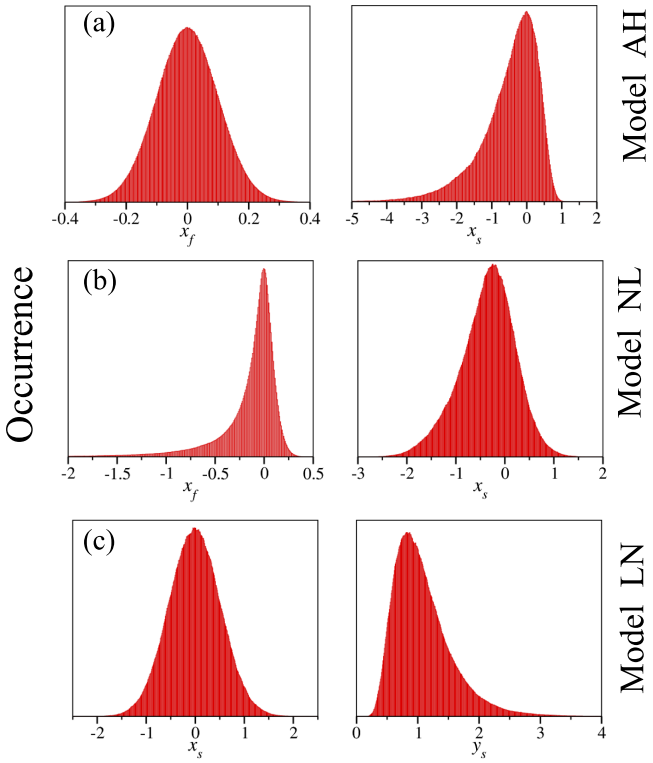

FIG. 1. The distribution of x_f (left) and x_s (right) for model AH (a) and model NL (b). (c) The distribution of x_s (left) and y_s (right) for model LN.

was employed to calculate the linear and two-dimensional (2DCS) spectra. This scheme relies on calculating the response functions governing the spectroscopic observables.[5] The real absorptive two-dimensional spectra were obtained as a sum of the rephasing and non-rephasing signals including ground state bleach, stimulated emission, and excited state absorption contributions.[64] This was done by solving the time-dependent Schrödinger equation for each 10 fs interval assuming that the Hamiltonian can be considered constant for such a short time. The time evolution for longer time-intervals can then be determined simply by multiplying the resulting time-evolution matrices successively on the wave function vectors. Strong coupling effects as included in the more elaborate hierarchy of equation of motion,[65] Ehrenfest,[66] and surface hopping[66,67] methods for simulating two-dimensional spectroscopy were not included. For the single chromophore systems studied here, this approximation essentially amounts to neglecting the effect of a possible Stokes shift.[8,23,66] In the present simulations, the overtone peak observed in 2DIR spectroscopy was moved out of the spectral window to simplify the analysis. Such peaks are typically absent or much weaker in 2DES spectroscopy. A homogeneous dephasing time of 50 ps was considered, which is larger than the bath correlation time. The correlation time, $\tau = \gamma/\kappa_s$, is 1.7 ps for the AH model and 5.5 ps for the NL and LN models. Thus, the homogeneous dephasing is expected to result in little motional narrowing of the linear spectra. The calculation of the spectra was done in the impulsive limit. In real experiments, pulse shapes have to be controlled carefully to avoid perturbing the spectral shapes.[8,68,69]

It is tempting to think that one can derive analytical expressions for the response functions in the log-normal case using a second-order cumulant approximation as the underlying dynamics is still Gaussian and, thus, fully described by the second-order cumulant of the underlying Gaussian dynamics. The present case is that we, however, did not find nice closed analytical expressions.

III. RESULTS AND DISCUSSION

A. Models with different physical origin of the skewness

The absorption spectra were calculated for the three models and the results are presented in Fig. 2. As can be seen, the absorption spectra, as expected, are asymmetric for all three models with a tail extending toward higher frequencies. Figure 2 shows that the three models are remarkably similar and they look very much like a log-normal distribution. We fitted the linear absorption spectra with a normalized intensity to a log-normal distribution, i.e.,

$$A(\omega) = \exp\left[-\frac{(\ln(\omega-\omega_0)-\mu)^2}{2\sigma^2}\right], \tag{12}$$

where μ and σ are the free parameters of the fit, while ω_0 is fixed (see Table II). The parameters obtained are given in Table II along with the skewness, which is derived from the fit parameters using

$$\Upsilon = \left(e^{\sigma^2}+2\right)\sqrt{e^{\sigma^2}-1}. \tag{13}$$

The data in Table II show that the skewness is very similar for the three models.

To obtain dynamical information about the three models, the real absorptive two-dimension (2D) spectra are computed as a sum of the rephasing and non-rephasing contributions, and the results for four-selected waiting times are shown in Fig. 3. As is seen, the 2D spectra for the three models are qualitatively similar. At $T = 0$ fs, the peaks are asymmetrically elongated along the diagonal axis, as they are in the linear absorption spectra. Then, as the waiting time increases, the peak spreads along the anti-diagonal axis, and at $T = 7$ ps, it becomes nearly triangular. The spectral shapes in Fig. 3 imply that at an early delay time, the correlation time is longer than the waiting time; consequently, there is a correlation between the excitation and the detection frequencies. This gives rise to a narrow peak along the anti-diagonal axis. As the waiting

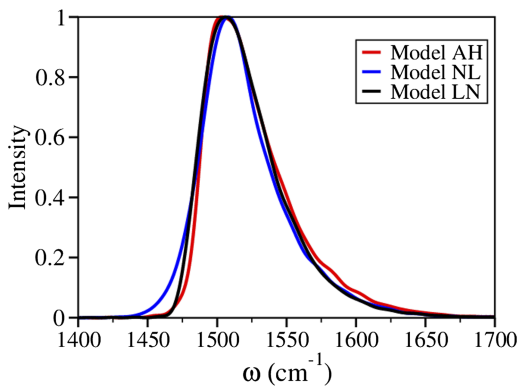

FIG. 2. The linear absorption spectra as computed with the NISE scheme.

TABLE II. The fitted parameters of the linear absorption line shape.

Model	μ	σ	ω_0	Υ
Model AH	4.12	0.37	1446.0	1.20
Model NL	4.03	0.41	1450.0	1.36
Model LN	4.02	0.42	1450.0	1.40

time increases, it becomes longer than the correlation time; as a result, no correlation is expected between the excitation and the detection frequencies. It is known that in the case of a Gaussian model, this gives rise to a circular peak.[12,60] In the current study, however, all three models result in triangular peak shapes. This triangular line shape can be understood as the product of the linear absorption spectra.[70] The observation that the spectra in Fig. 3 all behave in a very similar way indicates that it is meaningful to try to understand the peak shapes in terms of the simplest of the three. These results, thus, suggest that the log-normal model may be sufficient to analyze two-dimensional spectra in the presence of skewed distributions in general.

To get deeper insight into the dynamics observed in Fig. 3, the maxline slope as a function of waiting time is investigated. The maxline (see Fig. 3) is the line obtained by plotting the value of the detection frequency, where the intensity is the highest for a particular value of the excitation frequency. The slope of the maxline as a function of waiting time allows us to connect the 2D spectra with the two-point frequency fluctuation correlation function (FFCF), which is defined as

$$M(t) = C(t)/C(0) = \langle \delta\omega(0)\delta\omega(t)\rangle \,/\, \langle \delta\omega(0)\delta\omega(0)\rangle, \quad (14)$$

where $\delta\omega(t) = (\omega(t)) - \langle(\omega(t))\rangle$ which is used to characterize the memory of the bath dynamics. The two-point FFCF can be calculated directly from the Langevin simulation trajectories [see Fig. 4(a)]. The FFCF is, however, not an experimental observable. In practice, the dynamics observed in 2DCS are often analyzed using the maxline slope as a function of waiting time [see Fig. 4(b)]. Due to motional narrowing, the initial values of the maxline slope analysis are typically below unity, but at longer waiting times, the maxline slope and the FFCF are expected to be similar. To determine the time scale of the dynamics, we fitted the decays of the FFCF and the maxline slope in Fig. 4 according to a mono-exponential function. For the FFCF data, we find that the correlation times are 5.2, 6.3, and 5.0 ps for AH, NL, and LN models, respectively. For the maxline slope data [Fig. 4(b)], on the other hand, the correlation times obtained for model AH, model NL, and model LN are 2.8, 3.1, and 4.6 ps, respectively. We notice that the correlation time obtained from the FFCF and the maxline slope matches only for the LN model. This indicates that the maxline slope is not a good measure for the solvent dynamics for the case of non-Gaussian dynamics.

While the maxline slope analysis provides useful information about the memory of the bath, no clear additional information on the non-Gaussian dynamics is apparent for the present models. This is in contrast to a previous study

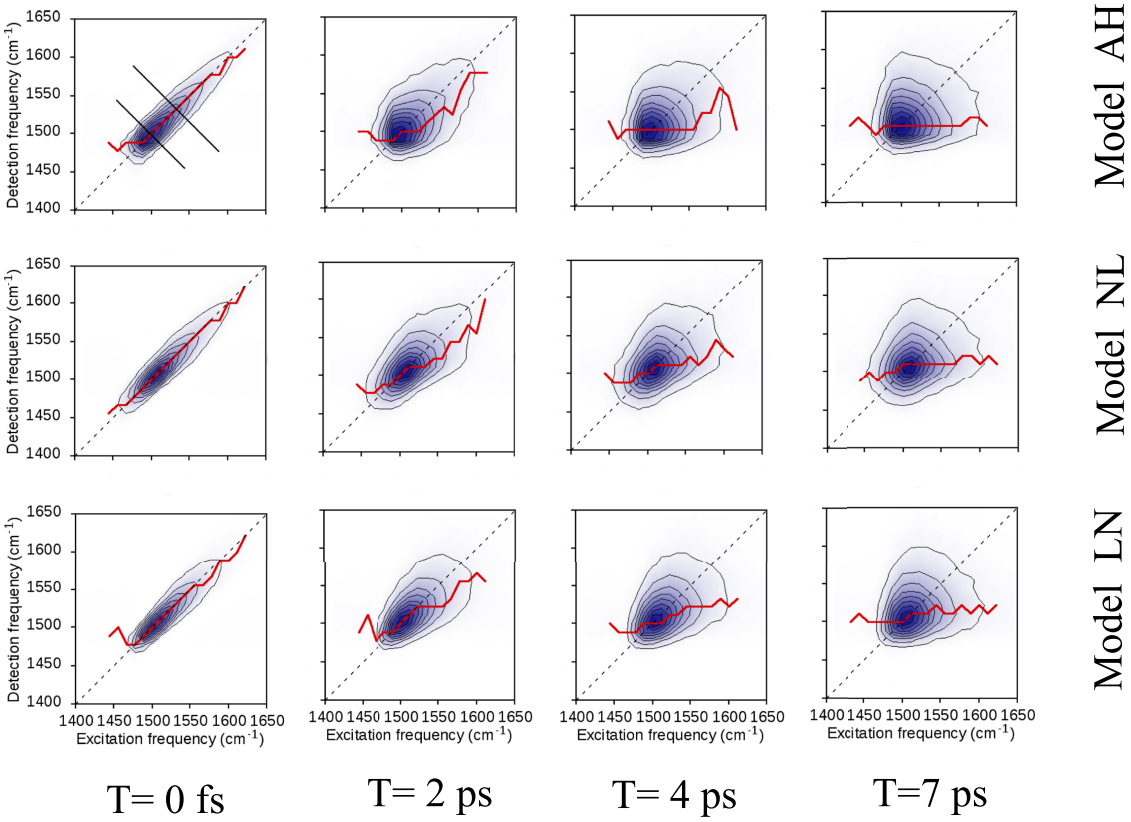

FIG. 3. The real absorptive two-dimensional (2D) spectra for the three models. The red line indicates the maxline, while the black lines refer to the anti-diagonal traces. The contours are plotted at 10% intervals of the normalized spectral amplitude. A dashed line indicates the diagonal.

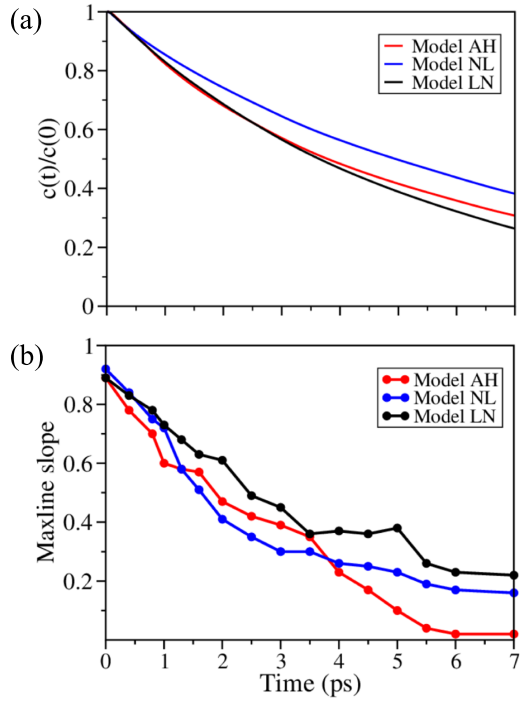

FIG. 4. (a) The calculated two-point FFCF of the frequency trajectory obtained directly from the Langevin simulation trajectories. (b) The maxline slope as a function of waiting time.

with a different type of model, where the maxline curvature was found to reveal information on the third-order frequency correlation function revealing the non-Gaussian nature of the dynamics.[12] From the spectra in Fig. 3, however, it is apparent that the 2D spectra spread along the anti-diagonal direction results in a triangular peak. Thus, we analyze the anti-diagonal widths as a function of waiting time to investigate the line shape of the 2D spectra. To calculate the anti-diagonal widths, two different traces along the anti-diagonal direction are considered, as depicted in Fig. 3. These traces are selected such that the first slice is centered at 1500 cm^{-1}, and the second slice is centered at 1533 cm^{-1}. To analyze the time evolution of the anti-diagonal widths, the full-width-at-half-maximum (FWHM) is calculated as a function of waiting time, and the results are presented in Fig. 5. As seen, a clear split is observed between the two slices for the three models. The difference in anti-diagonal linewidth increases as the waiting time increases.

B. Analysis of spectra for log-normal models with different skewness

To understand the effect of the skewness induced by the skewed models on the splitting noted in Fig. 5, we construct log-normal models with different skewness values and compare them with a Gaussian model where the skewness is zero (see Table III). The models are denoted as Gauss, log-normal I, and log-normal II. Here, Gauss refers to a Gaussian model, while log-normal I and log-normal II are two log-normal models, log-normal I with $\varrho = 0.04$ and $\eta = 1.0$ and log-normal II with $\varrho = -0.924$ and $\eta = 2.7$. The average frequency of the three models is centered at 1500 cm^{-1}. The skewness ($\langle\delta\omega(0)^3\rangle/\langle\delta\omega(0)^2\rangle^{3/2}$) and the variance ($\langle\delta\omega(0)^2\rangle$) calculated

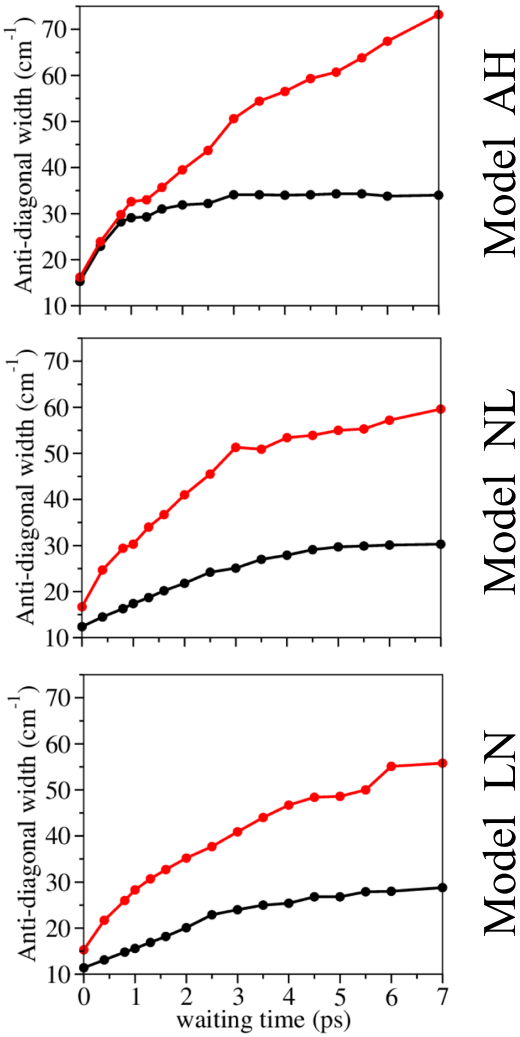

FIG. 5. The anti-diagonal widths as a function of waiting times. Black lines correspond to the traces centered at 1500 cm^{-1}, while red lines refer to those centered at 1533 cm^{-1}.

for these models from the Langevin simulations are presented in Table IV. The three models have similar variance and different skewness. In addition, the skewness for the log-normal II model is approximately three times higher than that for the log-normal I model.

To obtain dynamical information about the three models (Gauss, log-normal I, and log-normal II), the FFCF and the maxline slope are analyzed. The results are presented in Fig. 6, which show that the FFCF and the maxline slope for the Gaussian, log-normal I, and log-normal II models are similar and that it is impossible to distinguish between the Gaussian and

TABLE III. The values of the parameters used for the numerical calculation of the Gaussian, log-normal I, and II models.

Parameter	Value
k_s	0.133 J/m^2
m	20 amu
T	300 K
γ	5.50 ps^{-1}
c_s	150 cm^{-1}/nm

TABLE IV. The skewness and the variance that are calculated from the frequency trajectories.

Model	Skewness	Variance
Gauss	0.0	700.4
Log-normal I	0.5	708.7
Log-normal II	1.6	699.9

the log-normal models from the FFCF and the maxline slope. By fitting the curves in Fig. 6 to a mono-exponential function, we find that for the FFCF data, the correlation times obtained are 1.39, 1.38, and 1.32 ps for Gaussian, log-normal I, and log-normal II models, respectively. For the maxline slope data, the correlation time obtained for the Gaussian, log-normal I, and log-normal II models is 1.25, 1.24, and 1.20 ps, respectively. Thus, the correlation times obtained from the FFCF and the maxline slope are very close. Moreover, the correlation time obtained for the Gaussian model is very similar to the correlation time for the log-normal models. We suggest that if the system under study exhibits log-normal dynamics, we can determine both the time scale of the dynamics and the skewness from the FFCF by fitting the curve using[71]

$$C_l(t) = \exp\left[2\mu + \sigma^2\right]\left(\exp\left[\sigma^2\, C_g(t)\right] - 1\right), \tag{15}$$

where

$$C_g(t) = A\exp(-t/\tau). \tag{16}$$

Here, $C_g(t)$ corresponds to the correlation function of the Gaussian model which is used to construct the log-normal model. The results obtained from the fit using Eq. (15) are presented in Table V. The graphs in Fig. 6 are well fitted when we fix $\sigma = 0.17$ and 0.47 for log-normal I and log-normal II,

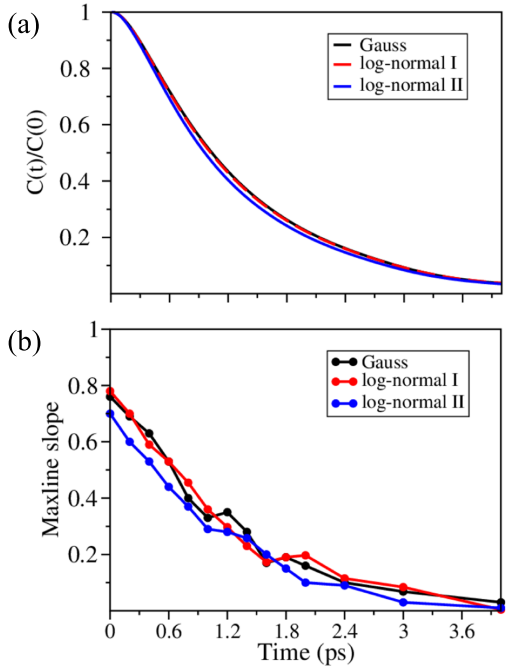

FIG. 6. (a) The calculated two-point FFCF of the frequency trajectory obtained from the Langevin simulations for the Gaussian model and the two log-normal models with different skewness. (b) The maxline slope as a function of waiting time for the three models.

TABLE V. The fitted parameters of the correlation function obtained from the FFCF and the maxline slope using Eqs. (15) and (16).

	FFCF				Maxline slope			
Model	A	τ (ps)	μ	σ	A	τ (ps)	μ	σ
Gauss	1.0	1.39	...	...	0.8	1.25	...	...
Log-normal I	1.0	1.39	1.77	0.17	0.8	1.25	1.76	0.17
Log-normal II	1.0	1.39	0.62	0.47	0.8	1.25	0.55	0.47

respectively, and leave μ to be a free parameter of the fit. The values of σ are chosen to produce the skewness in Table IV [see Eq. (13)]. The advantage of Eq. (15) is that it characterizes the log-normal dynamics. However, we should mention that the fit using Eq. (15) is not unique and Eq. (15) can be used to fit the curve of the Gaussian model as well. Although the 2D spectra for the Gaussian and log-normal models are different, the results of the maxline slope cannot distinguish between the Gaussian and log-normal models. Furthermore, the maxline slope for the log-normal models with different skewness is similar.

The results of the 2D spectra and the analysis for the anti-diagonal width as a function of waiting times are presented in Fig. 7. The latter shows that for the Gaussian model, the two graphs are almost coincident; by contrast, for the log-normal cases, the two graphs bifurcate and the distance between the two lines in Fig. 7 (middle panel) becomes larger when the skewness increases. Figure 8 shows that there is a linear relationship between the skewness and the splitting observed when analyzing the anti-diagonal width as a function of waiting time.

The effect of spectral diffusion on the 2D spectra for the three models is analyzed by calculating the joint probability density (JPD), and the data are compared with the 2D spectra obtained numerically. The 2D Gaussian joint probability density is defined as[26]

$$P(\delta\omega_3, T|\delta\omega_1, 0) = \frac{1}{2\pi\sigma^2(1-M^2(T))^{1/2}}$$

$$\exp\left(-\frac{\delta\omega_1^2 + \delta\omega_3^2 + 2M(T)\delta\omega_1\delta\omega_3}{2\sigma^2(1-M^2(T))}\right), \tag{17}$$

where $M(T)$ is the time dependent correlation coefficient [see Eq. (14)] which is varied between zero and one. $\delta\omega_1$ and $\delta\omega_3$ refer to the excitation and detection frequencies, respectively, in the 2D spectra. The 2D log-normal joint probability density, on the other hand, is given by

$$P(\delta\omega_3, T|\delta\omega_1, 0) = \frac{1}{2\pi\sigma^2(1-M^2(T))^{1/2}} \times \exp\left(\frac{q}{2\,(1-M^2(T))}\right),$$

$$q = \frac{(\ln(\delta\omega_1)-\mu)^2}{\sigma^2} - 2M(T)\frac{(\ln(\delta\omega_1)-\mu)}{\sigma} \times \frac{(\ln(\delta\omega_3)-\mu)}{\sigma} + \frac{(\ln(\delta\omega_3)-\mu)^2}{\sigma^2}. \tag{18}$$

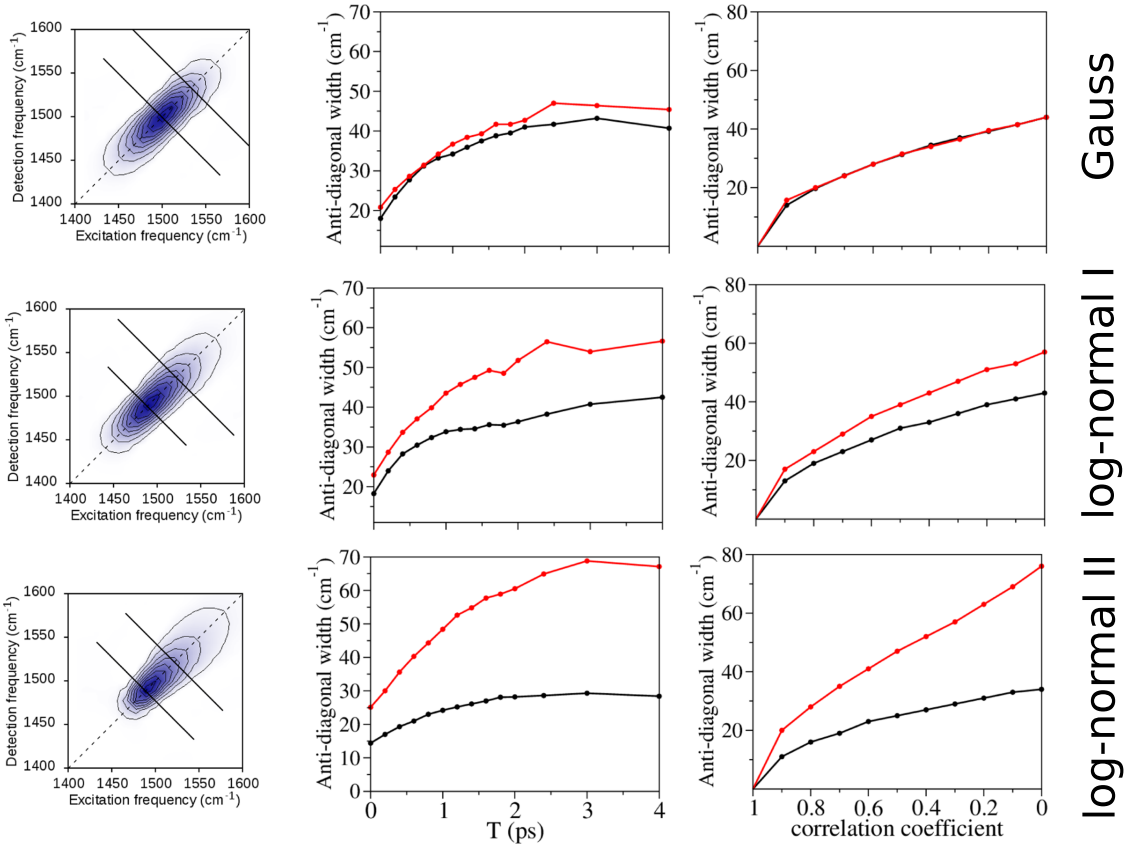

FIG. 7. Left panel: 2D spectra at $T = 0$ fs; the solid lines indicate the anti-diagonal traces. Middle panel: the anti-diagonal widths as a function of waiting time T. Right panel: The anti-diagonal widths calculated from the joint probability density [see Eqs. (17) and (18)]. Black lines correspond to the traces centered at 1489 cm^{-1}, while red lines refer to those centered at 1522 cm^{-1}.

One will expect the analytical JPD to match the simulated two-dimensional spectra fairly well, when the spectral dynamics during the coherence times is negligible. In practice, for short waiting times, the antidiagonal width will vanish in the JPD, while it is finite in experiments and numerical simulations. To calculate the 2D spectra from the JPD, the parameters σ and μ are taken from Table IV. The anti-diagonal widths are, then, calculated from the 2D spectra obtained from the JPD, and the results are displayed in Fig. 7 (right panel).

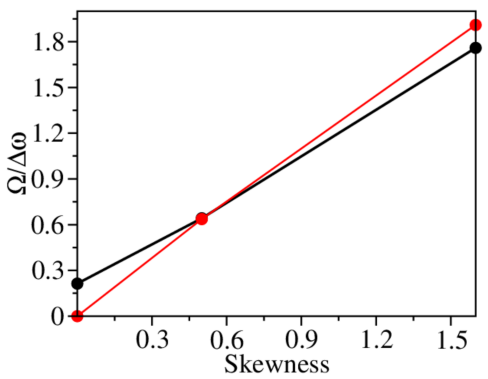

FIG. 8. The relationship between the skewness and the difference between the two traces of the anti-diagonal width at T = 4 ps (Ω) (the correlation coefficient is zero) divided by the frequency distance ($\Delta\omega$) between the two slices (see Fig. 7). The black line represents the data obtained from the numerical 2D spectra and the red line is the data obtained from the joint probability density.

Because of the motional narrowing in the case of the calculated 2D spectra, the initial values at $T = 0$ fs [see Fig. 7 (middle panel)] are larger than zero. In addition, we notice that the two graphs of the anti-diagonal widths obtained from the analysis of the analytical 2D spectra bifurcate as the correlation coefficient decreases, and that the distance between them increases when the skewness increases (see Fig. 8). Thus, they are very similar to those obtained from the numerically calculated 2D spectra. This indicates that the motional narrowing effect is minimal and that the JPD and the 2D spectra eventually reach the product line shape of excitation and detection frequency.[70]

C. Third-order correlation functions

To further examine the effect of the different origins of the skewness, we calculate the third-order correlation functions for the AH, NL, and LN models. The three-point FFCF is defined as

$$C_3(t_1, t_2) = \langle \delta\omega(0)\delta\omega(t_1)\delta\omega(t_2)\rangle. \tag{19}$$

For $t_1 = t_2 = 0$, this is equal to the skewness, when normalized with a factor $\langle \delta\omega(0)^2\rangle^{3/2}$, where $\langle \delta\omega(0)^2\rangle$ is the standard deviation. The diagonal elements of $C_3(t_1, t_2)$ can be simplified to a single time correlation function as

$$C_{11}(t_1) = \frac{\left\langle \delta\omega(0)\delta\omega^2(t_1)\right\rangle}{\langle \delta\omega(0)^2\rangle^{3/2}}. \tag{20}$$

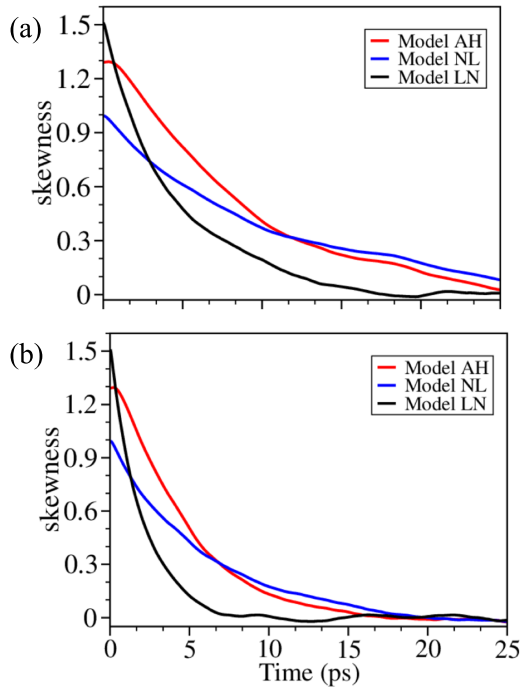

FIG. 9. The three-point FFCF of the frequency trajectory obtained from the Langevin simulation. (a) represents $C_{11}(t_1)$ and (b) refers to $C_{12}(t_1)$.

For Gaussian dynamics, $C_3(t_1, t_2)$ is identically zero at all times. This statement is limited to a simple Gaussian model in the weak coupling limit, where, for example, a Stokes shift can be neglected. The deviation from zero is, thus, a direct measure of the non-Gaussianity of dynamics. The three-point FFCF, $C_{11}(t_1)$, for our models is calculated and the results are presented in Fig. 9(a). In general, the AH, NL, and LN models have non-zero initial values, and within 20 ps, they decay to zero. The initial values in Fig. 9 are the skewness, and they are very close to those obtained from fitting the linear absorption spectra (see Table II). In addition, we calculated

$$C_{12}(t_1) = \frac{\langle \delta\omega(0)\delta\omega(t_1)\delta\omega(2t_1)\rangle}{\langle \delta\omega(0)^2\rangle^{3/2}}, \tag{21}$$

and the results are shown in Fig. 9(b). As seen, the graphs in Fig. 9(b) decay faster than the graphs in Fig. 9(a). Our analysis shows that the graphs in Fig. 9(b) can be reproduced from the graphs in Fig. 9(a) by multiplying the time with a factor of 1.75 for the AH and NL models and a factor of 2.1 for the LN model. This suggests that one can potentially distinguish the AH and NL models from the LN model using three-dimensional correlation spectroscopy, which is sensitive to the third-order correlation functions.[60]

IV. CONCLUSION

We employed model calculations to investigate the effect of frequency distribution skewness on the spectral line shape in linear absorption and two-dimensional correlation spectroscopy. We compared results from three different types of models, one where the non-Gaussian dynamics originates from anharmonicity in the bath potential, one where it originates from non-linear couplings in the bath, and a more phenomenological model where the non-Gaussian dynamics is constructed to have log-normal dynamics. We found that at an early delay time, the peak is asymmetrically elongated along the diagonal axis, and at long waiting times, the peak spreads along the anti-diagonal direction and gives rise to a triangular peak. This line shape is attributed to the skewness induced by the underlying dynamics. A triangular line shape does not automatically imply that the dynamics should be described with a log-normal model as other phenomena give rise to triangular peak-shapes.[70] We then analyzed the 2D line shape in terms of the maxline slope and the anti-diagonal widths for the three models as a function of waiting time. We found that the maxline slope allows extracting information about the correlation time, as is the case for Gaussian dynamics, and that the anti-diagonal widths reveal the skewness of the underlying dynamics. Moreover, the anti-diagonal width can distinguish the present models from standard Gaussian models. Our results suggest that a simple log-normal model is sufficient to study the dynamics of systems with skewed frequency distributions, where the origin of the skewness lies in anharmonicity or non-linear coupling in the bath. The key to understanding these spectra is, thus, the skewness, and other details of the models cannot be extracted with two-dimensional spectroscopy. Therefore, the origin of the skewed dynamics cannot be distinguished by two-dimensional spectroscopy, but calculated third-order correlation functions suggest that three-dimensional correlation spectroscopy, sensitive to this quantity, may be able to distinguish the anharmonic and nonlinear models from the log-normal one.

[1] J. D. Hybl, A. W. Albrecht, S. M. G. Faeder, and D. M. Jonas, Chem. Phys. Lett. **297**, 307 (1998).
[2] P. Hamm, M. H. Lim, and R. M. Hochstrasser, J. Phys. Chem. B **102**, 6123 (1998).
[3] R. R. Ernst, G. Bodenhausen, and A. Wokaun, *Principles of Nuclear Magnetic Resonance in One and Two Dimensions* (Oxford University Press, New York, 1995).
[4] P. Hamm and M. T. Zanni, *Concepts and Methods of 2D Infrared Spectroscopy* (Cambridge University Press, Cambridge, 2011).
[5] S. Mukamel, *Principles of Nonlinear Optical Spectroscopy* (Oxford University Press, New York, 1995).
[6] O. Golonzka, M. Khalil, N. Demirdöven, and A. Tokmakoff, J. Chem. Phys. **115**, 10814 (2001).
[7] K. Okumura, A. Tokmakoff, and Y. Tanimura, Chem. Phys. Lett. **314**, 488 (1999).
[8] J. D. Hybl, Y. Christophe, and D. M. Jonas, Chem. Phys. **266**, 295 (2001).
[9] K. Kwac and M. Cho, J. Phys. Chem. A **107**, 5903 (2003).
[10] S. T. Roberts, J. J. Loparo, and A. Tokmakoff, J. Chem. Phys. **125**, 084502 (2006).
[11] A. G. Dijkstra, T. L. C. Jansen, and J. Knoester, J. Chem. Phys. **128**, 164511 (2008).
[12] S. Roy, M. S. Pshenichnikov, and T. L. C. Jansen, J. Phys. Chem. B **115**, 5431 (2011).
[13] S. Woutersen, Y. Mu, G. Stock, and P. Hamm, Chem. Phys. **266**, 137 (2001).
[14] Y. S. Kim and R. M. Hochstrasser, Proc. Natl. Acad. Sci. U. S. A. **102**, 11185 (2005).
[15] Y. S. Kim and R. M. Hochstrasser, J. Phys. Chem. B **110**, 8531 (2006).
[16] F. Sanda and S. Mukamel, J. Chem. Phys. **125**, 014507 (2006).
[17] C. Scheurer and T. Steinel, ChemPhysChem **8**, 503 (2007).
[18] T. L. C. Jansen and J. Knoester, J. Chem. Phys. **127**, 234502 (2007).
[19] J. F. Cahoon, K. R. Sawyer, J. P. Schlegel, and C. B. Harris, Science **319**, 1820 (2008).
[20] R. Kubo, J. Phys. Soc. Jpn. **17**, 1100 (1962).
[21] R. Kubo, J. Math. Phys. **4**, 174 (1963).
[22] S. Mukamel, Phys. Rev. A **28**, 3480 (1983).

[23]F. Sanda, V. Perlik, C. N. Lincoln, and J. Hauer, J. Phys. Chem. A **119**, 10893 (2015).
[24]K. Lazonder, M. S. Pshenichnikov, and D. A. Wiersma, Optics Lett. **31**, 3354 (2006).
[25]D. G. Osborne and K. J. Kubarych, J. Phys. Chem. A **117**, 5891 (2013).
[26]S. Garrett-Roe and P. Hamm, J. Chem. Phys. **128**, 104507 (2008).
[27]T. L. C. Jansen, D. Cringus, and M. S. Pshenichnikov, J. Phys. Chem. A **113**, 6260 (2009).
[28]S. Garrett-Roe and P. Hamm, Acc. Chem. Res. **42**, 1412 (2009).
[29]F. van Mourik, M. Chergui, and G. van der Zwan, J. Phys. Chem. B **105**, 9715 (2001).
[30]C. Olbrich, T. L. C. Jansen, J. Liebers, M. Aghtar, J. Strümpfer, K. Schulten, J. Knoester, and U. Kleinekathöfer, J. Phys. Chem. B **115**, 8609 (2011).
[31]J. R. Schmidt, S. A. Corcelli, and J. L. Skinner, J. Chem. Phys. **123**, 044513 (2005).
[32]S. A. Corcelli, C. P. Lawrence, and J. L. Skinner, J. Chem. Phys. **120**, 8107 (2004).
[33]K. Kwac, H. Lee, and M. Cho, J. Chem. Phys. **120**, 1477 (2004).
[34]J.-H. Ha, K.-K. Lee, K.-H. Park, J.-H. Choi, S.-J. Jeon, and M. Cho, J. Chem. Phys. **130**, 204509 (2009).
[35]T. L. C. Jansen and J. Knoester, J. Chem. Phys. **124**, 044502 (2006).
[36]T. Hayashi, W. Zhuang, and S. Mukamel, J. Phys. Chem. A **109**, 9747 (2005).
[37]M. F. DeCamp, L. DeFlores, J. M. McCracken, A. Tokmakoff, K. Kwac, and M. Cho, J. Phys. Chem. B **109**, 11016 (2005).
[38]M. H. Farag, A. Bastida, M. F. Ruiz-López, G. Monard, and F. Ingrosso, J. Phys. Chem. B **118**, 6186 (2014).
[39]M. H. Farag, J. Zúniga, A. Requena, and A. Bastida, J. Chem. Phys. **138**, 205102 (2013).
[40]C. J. Fecko, J. D. Eaves, J. J. Loparo, A. Tokmakoff, and P. L. Geissler, Science **301**, 1698 (2003).
[41]T. Steinel, J. B. Asbury, S. A. Corcelli, C. P. Lawrence, J. L. Skinner, and M. D. Fayer, Chem. Phys. Lett. **386**, 295 (2004).
[42]J. Bredenbeck, J. Helbing, and P. Hamm, Phys. Rev. Lett. **95**, 083201 (2005).
[43]L. M. Kiefer and K. J. Kubarych, J. Phys. Chem. Lett. **7**, 3819 (2016).
[44]D. B. Siano and D. E. Metzler, J. Chem. Phys. **51**, 1856 (1969).
[45]R. Schanz, V. Botan, and P. Hamm, J. Chem. Phys. **122**, 044509 (2005).
[46]D. Bingemann and N. P. Ernsting, J. Chem. Phys. **102**, 2691 (1995).
[47]J. T. Kennis, D. S. Larsen, K. Ohta, M. T. Facciotti R. M. Glaeser, and G. R. Fleming, J. Phys. Chem. B **106**, 6067 (2002).
[48]O. Rancova and D. Abramavicius, J. Phys. Chem. B **118**, 7533 (2014).
[49]P. van der Meulen, H. Zhang, A. M. Jonkman, and M. Glasbeek, J. Phys. Chem. **100**, 5367 (1996).
[50]M. D. Edington, R. E. Riter, and W. F. Beck, J. Phys. Chem. **100**, 14206 (1996).
[51]S. Das, A. Datta, and K. Bhattacharyya, J. Phys. Chem. A **101**, 3299 (1997).
[52]P. Changenet, H. Zhang, M. J. van der Meer, M. Glasbeek, P. Plaza, and M. M. Martin, J. Phys. Chem. A **102**, 6716 (1998).
[53]C. Wang, B. K. Mohney, B. B. Akhremitchev, and G. C. Walker, J. Phys. Chem. A **104**, 4314 (2000).
[54]O. Rancova, M. Jakučionis, L. Valkunas, and D. Abramavicius, Chem. Phys. Lett. **674**, 120 (2017).
[55]J. Aitchison and J. A. C. Brown, *The Lognormal Distribution* (Cambridge University Press, 1963).
[56]K. Sun, *Department of Physics* (University of Illinois at Urbana-Champaign, 2004).
[57]M. Dinpajooh and D. V. Matyushov, J. Phys. Chem. B **118**, 7925 (2014).
[58]T. L. C. Jansen and S. Mukamel, J. Chem. Phys. **119**, 7979 (2003).
[59]D. M. Packwood and Y. Tanimura, Phys. Rev. E **84**, 061111 (2011).
[60]P. Hamm, J. Chem. Phys. **124**, 124506 (2006).
[61]A. Anda, L. De Vico, T. Hansen, and D. Abramavičius, J. Chem. Theory Comput. **12**, 5979 (2016).
[62]A. Nitzan, *Chemical Dynamics in Condensed Phases: Relaxation, Transfer and Reactions in Condensed Molecular Systems* (Oxford University Press, Oxford, 2006).
[63]T. L. C. Jansen and J. Knoester, J. Phys. Chem. B **110**, 22910 (2006).
[64]T. L. C. Jansen and J. Knoester, Acc. Chem. Res. **42**, 1405 (2009).
[65]A. Ishizaki and Y. Tanimura, J. Phys. Soc. Jpn. **74**, 3131 (2005).
[66]C. P. v. d. Vegte, A. G. Dijkstra, J. Knoester, and T. L. C. Jansen, J. Phys. Chem. A **117**, 5970 (2013).
[67]R. Tempelaar, C. P. van der Vegte, J. Knoester, and T. L. C. Jansen, J. Chem. Phys. **138**, 164106 (2013).
[68]D. M. Jonas, Annu. Rev. Phys. Chem. **54**, 425 (2003).
[69]R. Tempelaar, A. Halpin, P. J. M. Johnson, K. Cai, R. S. Murphy, J. Knoester, R. J. D. Miller, and T. L. C. Jansen, J. Phys. Chem. A **120**, 3042 (2016).
[70]S. M. G. Faeder and D. M. Jonas, J. Phys. Chem. A **103**, 10489 (1999).
[71]G. Zhang and Z. Chen, J. Appl. Stat. **42**, 603 (2015).